

# Photometric search for short-period Jupiter-size exoplanets in open clusters NGC 884 and NGC 869

IQBAL, JAVED <sup>1</sup>; GODERYA, SHAUKAT <sup>2</sup>; AND MAHMOOD KHAN, FAZEEL <sup>3</sup>

- 1) Department of Space Sciences, Institute of Space Technology, Islamabad Expressway, Sector H DHA Phase II Islamabad, 44000, Pakistan, [iqbaljaved1921@gmail.com](mailto:iqbaljaved1921@gmail.com)
- 2) Department of CHGP, Tarleton State University, 1333 W Washington St, Stephenville Tx, 76401, United States, [Goderya@tarleton.edu](mailto:Goderya@tarleton.edu)
- 3) Center for Astrophysics and Space Science, New York University Abu Dhabi, Saadiyat Marina District, Abu Dhabi, 129188, United Arab Emirates, [fmk5060@nyu.edu](mailto:fmk5060@nyu.edu)

**Abstract:** We present the results of a photometric survey aimed to detect short-period Jupiter-sized exoplanets in the open clusters NGC 884 and NGC 869. The survey was carried out over 11 non-consecutive nights using the 0.8-meter telescope at Tarleton State University, during which the central regions of the clusters were observed in the VBR filters for a total of 30.5 hours. Light curves were extracted from the time series data using the difference image subtraction package (ISIS 2.0) and a variability search toolkit (VaST). To search for potential exoplanet transit candidates, we applied a box least-squares algorithm to the light curve data, but no exoplanet candidates were identified. However, we were able to confirm 21 known variable stars and discover 4 new potential variable star candidates. The period analysis of the variable stars was performed using the NASA Periodogram service based on the Lomb-Scargle algorithm and a Lightcurve analysis tool based on the Lafler-Kinman algorithm.

## 1 Introduction

Since the discovery of the first exoplanet, to date, 5535 exoplanets have been confirmed. However, our understanding of planet formation as a function of stellar mass and environment remains limited, as the majority of these exoplanets have been found around isolated field stars. It has also been found that giant planets orbit metal-rich main sequence stars (Santos, Israelian, & Mayor 2004), while evolved stars that host giant planets are not metal-rich (Pasquini et al. 2007). This suggests that stellar metallicity plays a significant role in both planet formation mechanisms and the subsequent migration of planets towards their host stars. Stellar clusters offer an ideal laboratory to investigate these relationships, as they contain a large number of stars that have the same age, distance, and chemical composition, as they all formed from the same molecular cloud of gas. Furthermore, their homogeneous stellar environment allows direct comparisons between stars with and without planets. This further allows to assess whether the presence of planetary companions influences the metallicity of their host stars or not, which could provide insights into the conditions of planet formation into different stellar environments.

The number of exoplanets discovered in open clusters (OCs) has been increasing exponentially, with around 30 confirmed to date. Previous studies have reported the detection of various exoplanets in several OCs, including two sub-stellar companions in NGC 2423 and NGC 4349 (Lovis & Mayor 2007), two sub-Neptune orbiting a Sun-like star in NGC 6811 (Meibom et al. 2013), a non-transiting hot Jupiter in the Hyades (Quinn et al. 2014), five Jupiter-size exoplanets in the M67 OC (Brucalassi et al. 2017; Brucalassi, Pasquini, & Saglia 2016; Brucalassi et al. 2014), a Neptune-sized transiting planet in the Hyades (Mann et al. 2016), a Neptune-sized planet in M44 (Obermeier et al. 2016), seven transiting planets in the K2 campaign of M44 (Barros, Demangeon, & Deleuil 2016; David et al. 2016; Libralato et al. 2016), a sub-Neptune in NGC 6774 (Curtis et al. 2018), a Neptune-sized planet around a binary system in the Hyades (Ciardi et al. 2017), and three transiting planets in the Hyades (Livingston et al. 2018). Nardiello et al. (2020) reported the discovery of 11 exoplanet candidates, 7 of which are Jupiter-sized, in a survey of a young OC in the southern hemisphere. Furthermore, 11 new exoplanet candidates were identified in a radial velocity survey conducted to search for exoplanets in young OCs with solar metallicity stars (Leão et al. 2018). These findings confirm the presence of exoplanets in OC environments.

The double clusters NGC 884 and NGC 869 are very young, moderately dense, and brightest OCs located in the northern hemisphere, in the constellation of Perseus. In terms of fundamental physical parameters, these two clusters are nearly identical. The double cluster has an age range of 10–20 million years, a distance modulus between 11.6–11.8, and a reddening 0.4–0.6 (Currie et al. 2010). These characteristics of double clusters make them ideal candidates for studies of stellar populations and the potential detection of exoplanets. The double cluster has been extensively studied for variable stars and has yielded the detection of several variable stars. Previous variability studies in the OCs NGC 884 and NGC 869 have reported the detection of several variable stars and eclipsing binary systems. In NGC 884, Percy (1972) conducted a photometric study and discovered three variable stars. Waelkens et al. (1990) conducted a long-term photometric study and reported several Be stars. Krzesinski and Pigulski (1997) reported the presence of two eclipsing binaries and six beta-Cepheid variables. An additional eclipsing binary was discovered by Ivashchenko and Golovin (2007). Saesen et al. (2010) carried out an extensive multi-site photometric campaign in NGC 884 and found six eclipsing binaries and four variable star candidates. Similar to the NGC 869 OC, Krzesinski, Pigulski, and Kolaczowski (1999) identified ten variable stars, including two eclipsing binaries. Two variable stars were identified by Majewska-Świerzbiniowicz et al. (2008). Most recently, Zhuo et al. (2021) detected eight variable stars and one eclipsing binary in the NGC 869 OC. However, no dedicated multi-wavelength photometric studies of exoplanets have been carried out in the double cluster.

## 2 Equipment and Observation

The observations were carried out using the remotely controlled telescope of Tarleton State University (TSU), located at 32° 13' 58.37" N, 98° 5' 51.46" W in Stephenville, Texas, at an elevation of 344 m. The TSU observatory is equipped with a 0.8-metre Ritchey-Chretien telescope and a Andor iKon-L CCD camera of 2048×2048 pixels, providing a field of view of 17' × 17' and a plate scale of 0.497 arcseconds per pixel. The original observing plan was to monitor both the OCs NGC 884 and NGC 869 for a total of 30 consecutive nights, with 15

nights dedicated to each cluster. However, due to unfavorable weather conditions during the scheduled observing window, the observations were ultimately limited to just 11 non-consecutive nights. During this observing period, the central region of NGC 884 was observed for 5 nights, for a total of 14.08 hours of integration time, while the NGC 869 was observed for 6 nights, resulting in 16.42 hours of data collection. The observations were carried out in VBR filters, resulting in a total of 6,609 CCD images for both clusters over the 30.5 hours of observation time. The seeing conditions during the observing campaign ranged from a minimum of 1.0 arcseconds to a maximum of 1.7 arcseconds, with a median value of 1.5 arcseconds. Further details of the observations are provided in Tables 1 and 2.

Table 1: Summary of the observations of NGC 884 OC, including the date, total observation time, and exposure time for each filter.

Observation date [UT]	Time-span [hours]	$B [T_{\text{exp}} \times N_{\text{img}}]$	$V [T_{\text{exp}} \times N_{\text{img}}]$	$R [T_{\text{exp}} \times N_{\text{img}}]$
19 November, 2020	3.18	20×255	15×255	10×255
21 November, 2020	2.53	20×203	15×203	10×203
17 December, 2020	3.27	20×262	15×262	10×262
20 December, 2020	2.51	20×201	15×201	10×201
21 December, 2020	2.57	20×206	15×206	10×206
Total	14.08	6.26	4.69	3.13

Table 2: Summary of the observations of NGC 869 OC, including the date, total observation time, and exposure time for each filter.

Observation date [UT]	Time-span [hours]	$B [T_{\text{exp}} \times N_{\text{img}}]$	$V [T_{\text{exp}} \times N_{\text{img}}]$	$R [T_{\text{exp}} \times N_{\text{img}}]$
18 November, 2020	5.5	30×360	15×360	10×360
20 November, 2020	2.96	30×194	15×194	10×194
07 December, 2020	1.40	30×92	15×92	10×92
10 December, 2020	2.53	30×166	15×166	10×166
18 December, 2020	2.49	30×163	15×163	10×163
22 December, 2020	1.54	30×101	15×101	10×101
Total	16.42	8.96	4.48	2.98

### 3 The Reduction Process

#### 3.1 The pre-reduction procedure

The calibration was performed using GCX Photometry and Reduction software, along with custom-written Python code specifically developed for the Tarletan observatory data. The process included bias, dark, and flat field calibration. First, the 20 bias frames were averaged to create a master bias, which was then subtracted from all raw frames to eliminate readout noise. Next, a master dark frame was generated and subtracted from both the master bias and raw images to account for the dark current. Finally, a dark median flat was created by combining

and normalizing all flat frames, correcting for pixel-to-pixel variations in sensitivity and vignetting caused by the telescope's optics.

After the calibration, we performed a visual inspection of the calibrated images to identify and remove images that were affected by various issues (saturated stars, low SNR, cosmic rays, and telescope tracking). In the NGC 884 dataset, we discard 81 B-filter, 50 V-filter, and 56 R-filter images due to various issues. Similarly, for NGC 869, we removed 70 B-filter, 35 V-filter, and 43 R-filter images. Additionally, we had to delete the entire dataset of NGC869 collected on December 22, as all the images were affected by intermittent cloud cover, resulting in a point-spread function greater than 10 pixels and sky levels exceeding 10,000 ADU. After this thorough review process, we were left with 1,071 high-quality R-filter, 1,077 V-filter, and 1,046 B-filter images of NGC 884, as well as 932 high-quality R-filter, 940 V-filter, and 905 B-filter images of NGC 869.

## 3.2 Data Reduction Strategies

We use two different methods for the data reduction: (1) Image subtraction photometry using ISIS 2.0, and (2) PSF fitting photometry using VaST. The brief description of each is given in the next section. The purpose of doing photometry with two different method was to confidence the result and compare the performance of each method.

### 3.2.1 Image Subtraction Photometry With ISIS

We used the difference image subtraction package ISIS 2.0, developed by (Alard 1998; Alard 2000). A composite reference image is constructed by averaging multiple best-seeing images together. Then Kernel is computed for each image, which describes the PSF across the image with respect to the reference image. The kernel is then convolved with the PSF of the reference image in order to match as closely as possible with each image, and the resulting reference image is subtracted from each individual image. On the subtracted image, only stars with significant variation are left, which are potential variability candidates. Then photometry is performed on the subtracted images.

We followed the standard reduction routine of ISIS 2.0. This began with aligning the images to the reference image in order to correct for small rotations and shifts. In most cases, the first image of the dataset was used as the reference image for astrometric transformation, except for data from November 17 and 20 of NGC 884 and December 18 of NGC 869, where different reference images were used. This was because the target was slightly off-center, which result in all images are not properly aligning. The composite reference image was then constructed by averaging the 20 best-seeing images in each filter. We tried the range of parameters values for the optimal image subtraction and find that dividing the image into four sub-regions and setting kernel value 12, stamp size 15 with second-order sky background variables gave the best results for our data. However, these parameters did not work for the B-filter data, and even using larger values caused program (ISIS 2.0) to crash after processing only a few images. We find that the short exposure times of the B-filter images made it difficult to properly identify sources and fit the background compared to the reference image. As a result, we decided not to use B-filter data in further analysis, and will focus only on the R and V-filter datasets.

After completing the image subtraction on the V and R-filter datasets, we conducted aperture photometry on the subtracted images and computed the differential flux for potential variable sources identified by ISIS 2.0. The light curves for these individual sources were then generated using the Gnuplot software. Through this analysis, we potentially identified a total of 45 variable sources in the V-filter dataset and 51 variable sources in the R-filter dataset of both OCs.

### 3.2.2 PSF Fitting Photometry with VaST

In contrast to the difference image subtraction, the VaST (Sokolovsky & Lebedev 2018) performed point-spread function fitting photometry. VaST is a widely used tool for detecting transient events and variable sources in large photometric datasets. It has been extensively tested on various datasets to detect planetary transits and variable stars and provide reliable results. The VaST analysis starts by stacking one of the best-seeing images as an astrometric and photometric reference image in the configuration file. We used the same reference images as in the ISIS analysis. A key advantage of VaST is that it requires only 40% image overlap with the reference image to perform accurate photometry, making it more efficient and flexible, especially for under-sampled datasets with limited image quality. VaST then computed various variability indices for each object with respect to the reference image and identified potential variable candidates based on these indices. Subsequently, it performed point-spread function fitting photometry on all individual objects, fitting a model PSF. This provides more accurate photometry than the aperture photometry with the ISIS. Then, it generated light curves for the variability candidates and provided valuable information, including object identification, magnitude calibrations, and cross-checking each object against variable star databases. The results from the VaST analysis generally agree well with the light curves obtained from the ISIS 2.0 analysis. In total, the VaST analysis identified 36 variable objects in the V-band and 42 in the R-band data for both OCs.

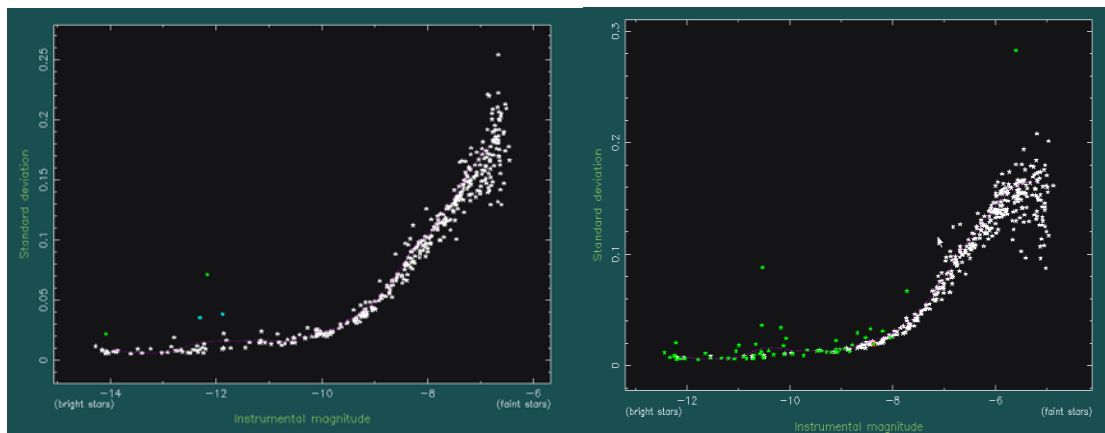


Figure 1: Shows the standard deviation of the light curves plotted against the instrumental V-band magnitude, measured over a five-day dataset for NGC884 (Right) and NGC869 (Left) in VaST dialog Window. The graph indicates that bright stars exhibit low standard deviations, likely due to their high SNR. In contrast, on the faint end, the background noise is dominant and shows large standard deviations.

### 3.2.3 Selection Criteria for Light Curves

We used the following criteria for the selection of the stars for the final analysis of light curves to achieve maximum confidence and reliability in the results: This included objects that were identified by both packages, had a good signal-to-noise ratio, magnitude variation greater than photometric sensitivity, and similar light curve variation observed in both filters. After applying these criteria, we were left with 25 potential variability candidates.

### 3.2.4 Search for Planetary Transit event

To search for planetary transit signals in our light curves, we first visually inspected all the light curves for possible transit signals. Then, we use the box least-squares algorithm of Aigrain and Irwin (2004) to search for potential transits in a more systematic way. We generate a transit model for a range of transit durations from 1 to 3 hours, with a step size of 0.25 hours. Each model is fitted over light curves, and a chi-squared value is calculated for each light curve. However, our analysis did not reveal any statistically significant transit signals that would be consistent with the transiting exoplanets. The lack of exoplanet detections in our data could be due to several factors. One possible explanation is that the planets orbiting these host stars may have relatively long orbital periods, requiring extended observation windows to fully capture a complete transit. The non-consecutive nature of our observation, with gaps in the data, has affected our ability to detect such long-period transits. Another possible reason could be that the transits are simply too shallow or frequent to be reliably identified in our data.

### 3.2.5 Period Analysis

For the period analysis, we use the light curves generated by the VaST software, which provided instrumental magnitudes. However, our dataset had certain limitations, such as undersampling and gaps, that prevented us from reliably converting the differential flux from the ISIS 2.0 photometry into standard magnitudes. Moreover, the PSF-fitting photometry was not effective in cases where stars were blended, further complicating the process of obtaining accurate zero-magnitude conversions from the instrumental magnitudes. Therefore, we were unable to obtain an accurate zero-magnitude conversion from the instrumental differential magnitude from VaST and ISIS 2.0 photometry. The period analysis on the light curves of the identified variable stars was performed using a web-based lightcurve analysis tool based on the Lafler-Kinman method (Lafler & Kinman 1965) and the NASA periodogram based on the Lomb-Scargle algorithm (Lomb 1976; Scargle 1982). They provide reliable periods for a wide range of variable star types, from short-period beta cepheid variables to long-period slow pulsating variables and eclipsing binaries. Through this analysis, we were able to determine the periods for 25 variable stars identified in the OCs NGC 884 and NGC 869. The period estimates obtained from our analysis show good agreement with previously published results for most of the variable stars.

## 4 Results

### 4.1 Variable Stars

We used a traditional approach to classify the newly identified variable stars, as well as those that had not been previously classified. This classification process was based on the shape of the light curve, periods, and the amplitude of variations. The variable stars were categorized into eclipsing binaries (EA), beta Cepheid ( $\beta$  Cep), Lambda ( $\lambda$  Eri), Slow pulsating B-type

(SPB), and long-period pulsating (LPP) stars. These variable stars were cross-checked against the General Catalogue of Variable Stars (GCVS) and the American Association of Variable Star Observers (AAVSO) database. The phase-folded light curves for all the variable stars are presented in the appendix. Table 3 provides key details, such as their WEBDA IDs, coordinates, periods, and variability types, for the variable stars detected in our field of view (FOV). The details are discussed in subsections below.

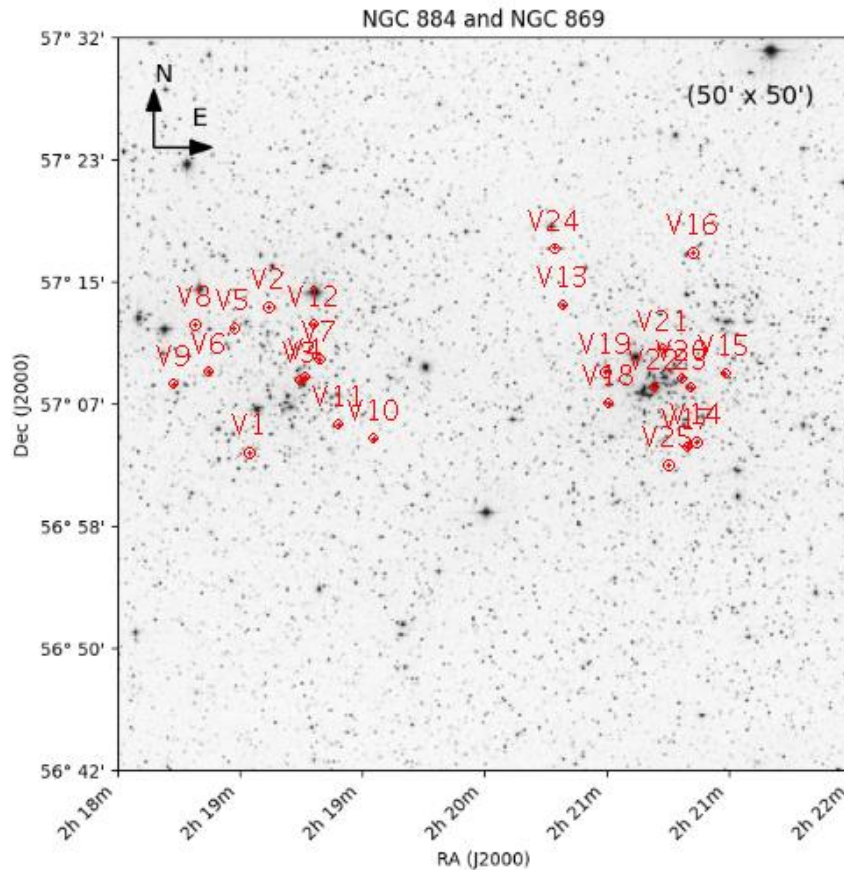


Figure 2: The variable stars identified in our FOV of the open clusters NGC 884 (right) and NGC 869 (left) are marked with circles and labelled with their serial number.

Table 3: Provide the necessary information of the variable star identified in our FOV.

Sr.No	WEDBA IDs	RA[d:m:s]	Dec [d:m:s]	Epoch [JDmax]	Period [days]	Cross IDs	Type	Cluster
V1	2433	02 22 27.43	+57 03 17.40	2459172.87300	0.9452±0.0001		EA	NGC884
V2	2351	02 22 15.81	+57 13 29.09		11.61		EA	NGC884
V3	2246	02 22 02.78	+57 08 25.02	2459174.81151	0.184±0.003	V619 Per	β Cep	NGC884
V4	2227	02 22 00.57	+57 08 41.87	2459174.75484	0.164±0.021	NSV 798	β Cep	NGC884
V5	2444	02 22 29.85	+57 12 28.84	2459174.75302	0.218±0.011	BD+56 584	β Cep	NGC884
V6	2572	02 22 48.96	+57 09 13.97	2459174.85504	0.222±0.004	BD+56 590	β Cep	NGC884
V7	2165	02 21 52.94	+57 09 58.94	2459203.51499	0.200±0.002	NSV 796	β Cep	NGC884
V8	2622	02 23 00.06	+57 12 13.97	2459205.71002	0.482±0.007		β Cep	NGC884
V9	2649	02 23 04.18	+57 07 38.78	2459174.70380	0.457±0.012		β Cep	NGC884
V10	2085	02 21 42.93	+57 05 30.61	2459174.77233	0.349±0.034		β Cep	NGC884
V11	2185	02 21 55.56	+57 05 58.65	2459203.67921	1.588±0.012		SPB	NGC884
V12	2191	02 21 58.94	+57 12 20.28	2459172.82207	2.014±0.216		SPB	NGC884
V13	1516	02 20 02.97	+57 11 18.68		1.732		EA	NGC869
V14	0803	02 18 42.77	+57 04 21.51	2459171.86858	0.105±0.017		β Cep	NGC869
V15	0692	02 18 29.83	+57 09 03.16	2459173.86858	0.170±0.001	BD+56 501	β Cep	NGC869
V16	0839	02 18 48.01	+57 17 07.88	2459171.58056	0.246±0.004	BD+56 508	β Cep	NGC869

V17	1001	02 19 00.38	+57 04 27.18	2459171.78122	0.253±0.005		β Cep	NGC869
V18	1282	02 19 28.82	+57 07 04.54	2459171.72141	0.532±0.041		β Cep	NGC869
V19	1268	02 19 27.46	+57 08 17.64	2459171.58056	0.368±0.005		β Cep	NGC869
V20	0893	02 18 51.12	+57 08 36.35	2459171.88402	1.451±0.027	V612 Per	SPB	NGC869
V21	1015	02 19 01.72	+57 10 43.14	2459174.85504	1.027±0.061		SPB	NGC869
V22	1057	02 19 04.42	+57 08 07.79	2459173.82300	2.891±0.053	BD+56 522	LPP	NGC869
V23	0922	02 18 53.86	+57 08 22.23	2459171.59821	0.274±0.013	V613 Per	λ Eri	NGC869
V24	1490	02 19 57.85	+57 17 33.72	2459173.82094	5.182±0.018		LPP	NGC869
V25	0847	02 18 47.93	+57 04 02.18	2459204.53743	7.624±0.036	BD+56 511	LPP	NGC869

## 4.2 Eclipsing binaries (EA)

In our FOV of both OCs, we identified a total of three eclipsing binaries. Two of them, WEBDA IDs 2433 and 2351, are in the NGC 884 OC, while one, 1516, is in the NGC 869 OC. Saesen, Carrier, and Pigulski (2009) discovered ID 2433 and characterized it as an Algol-type eclipsing binary with a period of 0.95 days. Guo et al. (2020) obtained a photometric solution and calculated a slightly shorter period of 0.9453 days. Using the Lafler and Kinman method, we calculated an even shorter period of 0.9452 days. We detected both primary and secondary minima in the data from November 19 and 21, while in the other three nights only small magnitude variations were observed. The other two Algol-type eclipsing binaries, ID 2351 with a period of 11.61 days and ID 1516 with a period of 1.732 days, had been previously reported by Saesen, et al. (2009) and Guo, et al. (2020) respectively. In our data, we observed only the primary minima of these two stars in a one night, while no clear magnitude variation was detected on the remaining four nights. Due to insufficient data, we were unable to accurately determine the periods of these two eclipsing binaries using our data. Therefore, we just phase-fold their light curves based on previously published periods. The phaser plots of all three systems are presented in appendix.

We also obtained photometric solution for the binary system ID 2433, using the Physics of Eclipsing Binaries (PHOEBE) software (Prša & Zwitter 2005). Initial estimates for parameters such as effective temperature, mass ratio and inclination angle were made based on the results of (Guo, et al. 2020). All other parameters were set free, and a synthetic light curve was obtained. Then, the parameters were adjusted to obtain a synthetic light curve that fits well over the observed data. Once a satisfactory fit was achieved, PHOEBE's optimization tool was used to further refine the light curve solutions. The best-fitted model over the observed data is shown in Figure 3. There is a minor difference between the observed data and synthetic models at a phase value of 0.1, but an excellent agreement at phase value of 0.9. This may be because data for the system was missing at this phase value. The final results derived from it are presented in Table 4. Our results are in good agreement with the previous findings, except the inclination angle and mass ratio which are slightly higher.

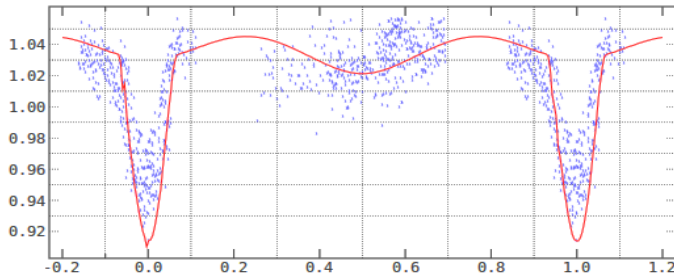


Table 4:  
Parameters of  
eclipsing  
binary 2433

Parameters	Values
Period (days)	$0.9452 \pm 0.004$
$T_1$ (K)	$7800 \pm 130$
$T_2$ (K)	$3790 \pm 180$
$i$ (deg)	$64 \pm 0.5$
$q$ ( $M_2/M_1$ )	$0.12 \pm 0.02$

Figure 3: The synthetic light curve (solid line) fitted over the observational data points with PHOEBE in the V-filter data

#### 4.3 Beta Cepheid ( $\beta$ Cep) Variable stars

Star IDs 2246, 2227, 2165, 2444, 2572, 2622, 2649, and 2085 were previously identified as beta-Cepheid variable stars in the NGC 884 OC (Krziesinski & Pigulski 1997; Saesen, et al. 2009; Saesen, et al. 2010; Laur et al. 2017). However, due to insufficient data, the periods for 2227, 2165, and 2085 had not been previously calculated. We recover the periods of the stars that were previously determined and also calculated the periods for 2227 and 2165 that were unknown and classified them as beta Cepheid variable stars with periods of 0.164 days and 0.200 days, respectively (see appendix, Table 3).

The star IDs 0692, 0839, 0803, and 1001 were also previously reported as beta Cepheid variable stars with periods of 0.1716 days, 0.242 days, 0.3 days, and 0.258 days, respectively, in NGC 869 OC (Krziesinski, et al. 1999; Gomez-Forrellad 2000; Labadie-Bartz et al. 2020; Zhuo, et al. 2021). For the stars with IDs 0692, 0839, and 1001, we were able to recover their previously reported periods. However, for the star with ID 0803, we found the period to be different from the previously published value. This was a single instance where our period was significantly different from the previous period. Our dataset indicates the period for this star is 0.105 days. We verified this period using the Lomb-Scargle Periodogram and could not detect any other significant frequencies. Additionally, we identified two new variable stars with IDs 1282 and 1268 in the FOV of NGC 869. Analysis revealed their periods to be 0.532 days and 0.368 days, respectively. For the star with ID 1268, the period, amplitude, and light curve shape suggest it is likely a beta Cepheid variable (see appendix, Table 3). The period and amplitude of the light curve of star ID 1282 suggest that it is also a possible beta Cepheid variable (see appendix). However, upon close inspection, the shape of the light curve for this star does not fully align with the typical beta Cepheid variables. Instead, the light curve shape appears more consistent with that of a W UMa-type contact binary system. Further observations and detailed investigation will be necessary to determine the true nature and proper classification of this star.

#### 4.4 Slow Pulsating B-type (SPB) variable stars

In addition to the beta Cepheid variable stars, we also identified four slowly pulsating B-type variable stars in our FOV of both OCs. The star with IDs 2185 and 2191 were found in the NGC 884 OC, while IDs 0893 and 1015 were identified in the NGC 869 OC. Three of these SPB variables, with IDs 2185, 2191, and 0893, had been previously reported by (Krziesinski & Pigulski 1997); Saesen et al. (2013) and (Labadie-Bartz, et al. 2020) with periods of 1.6 days, 2.23 days, and 1.47 days, respectively. We recovered the periods of these three stars (see appendix, Table 3). However, the star with ID 1015 had been previously noted as a variable, but its period could not be determined due to insufficient data, and no classification was provided. Our observations confirmed the variability of this star, and based on our analysis, the best estimated period for this star is 1.027 days, suggesting it is likely a slowly pulsating B-type variable.

#### 4.5 Lambda Eri ( $\lambda$ Eri) Variable star

We also identified one  $\lambda$  Eri variable star ID 0922 in our FOV of NGC 869. Krzesinski, et al. (1999) had previously discovered this star and reported its period as 0.287 days. However, our analysis calculated a slightly shorter period of 0.274 days (see appendix, Table 3). The  $\lambda$  Eri variables are a class of pulsating variable stars that show small amplitude variations and short periods, typically between 0.5 to 2 days. Despite the low-amplitude nature of the variations, we are confident that the magnitude variation observed in our dataset for this star is real and true because the maximum and minimum magnitude appear at the same time and have identical depth. A phased light curve is found in the appendix.

#### 4.6 Long period pulsating (LPP) variable stars

In addition, in our dataset, we identified three long-period variable stars with IDs 1057, 1490, and 0847. Star ID 1057 is in the FOV of NGC884, and the other two are in the FOV of NGC869. The star ID 1057 was previously reported as an irregular B-type variable by Krzesinski, et al. (1999), but we observed periodic variations in its light curve. The other two were not previously identified as variable stars, and no data was found about them in any variable star's database. We observed consistent variations across different filters and nights for all these stars in our dataset, which gives us confidence that the variations are real. However, our observation span was not long enough to accurately calculate the periods of these long-period variables. As a result, we can only provide approximate periods for them. Our estimated periods of these star IDs (1057, 1490, and 0847) are 2.891, 5.182, and 7.624 days, respectively, suggesting they are likely regular long period variables stars. The gap in the phased light curves is due to the limited observing window of this study. The phased folded light curves of these three long-period variable stars are presented in the appendix and period in Table 3.

## 5 Conclusion

In a photometric study of the OCs NGC 884 and NGC 869, we identified 25 variable stars, four of which are new potential variable star candidates (IDs 1282; 1268; 1490; 0847) with no evidence of exoplanet transits. These includes 3 EA, 14  $\beta$  Cep variables, 1  $\lambda$  Eri, 4 SPB, and 3 LPP variable stars. We determined the periods of these variable stars and classified them based

on the nature of their variability. The absence of exoplanet detections in these OCs does not necessarily mean that no planets exist in these clusters. However, further long-term, consecutive-night observations are required not only to search for exoplanets but also to better characterize the variable star populations, particularly the newly detected variables, and to understand their pulsation properties in more detail.

## Acknowledgement

We would like to express our gratitude to Tarleton State University for granting us telescope time for observation and other computational resources. This research has made use of the WEBDA database, operated at the Institute for Astronomy of the University of Vienna, SIMBAD database, operated at CDS, Strasbourg, France, GCVS operates by the Institute of Astronomy at the Russian Academy of Sciences, AAVSO, PHOEBE and NASA Periodogram.

## References

- Aigrain, S., & Irwin, M. 2004, MNRAS, 350, 331. [2004MNRAS.350..331A](#)
- Alard, C. 2000, A&A, 144, 363. [2000A&AS..144..363A](#)
- Alard, C., & Lupton, R. H. 1998, The Astrophysical Journal, 503, 325. [1998ApJ...503..325A](#)
- Barros, S., Demangeon, O., & Deleuil, M. 2016, A&A, 594, A100. [2016A&A...594A.100B](#)
- Brucalassi, A., et al. 2017, A&A, 603, A85. [2017A&A...603A..85B](#)
- Brucalassi, A., Pasquini, L., & Saglia, R. 2016, A&A592 L, 1. [2016A&A...592L...1B](#)
- Brucalassi, A., et al. 2014, A&A, 561, L9. [2014A&A...561L...9B](#)
- Ciardi, D. R., et al. 2017, arXiv, 170910398. [2018AJ....155...10C](#)
- Currie, T., et al. 2010, The Astrophysical Journal Supplement Series, 186, 19. [2010ApJS..186..191C](#)
- Curtis, J. L., et al. 2018, The Astronomical Journal, 155, 173. [2018AJ....155..173C](#)
- David, T. J., et al. 2016, The Astronomical Journal, 151, 112. [2016AJ....151..112D](#)
- Gomez-Forellad, J. 2000, Information Bulletin on Variable Stars, No 4924, # 1, 4924. [2000IBVS.4924....1G](#)
- Guo, D.-F., et al. 2020, MNRAS, 497, 3381. [2020MNRAS.497.3381G](#)
- Ivashchenko, G., & Golovin, A. 2007. in 14th Young Scientists Conference on Astronomy and Space Physics, 14th Young Scientists Conference on Astronomy and Space Physics. [2007ysc.conf....1I](#)
- Krziesinski, J., & Pigulski, A. 1997, A&A, v 325, p 987-993, 325, 987. [1997A&A...325..987K](#)
- Krziesinski, J., Pigulski, A., & Kolaczowski, Z. 1999, A&A, 505. [1999A&A...345..505K](#)
- Labadie-Bartz, J., et al. 2020, The Astronomical Journal, 160, 32. [2020AJ....160...32L](#)
- Lafler, J., & Kinman, T. 1965, Astrophysical Journal Supplement, vol 11, p 216 (1965), 11, 216. [1965ApJS...11..216L](#)
- Laur, J., Kolka, I., Eenmäe. 2017, A&A, 598, A108. [2017A&A...598A.108L](#)
- Leão, I., et al. 2018, A&A, 620, A139. [2018A&A...620A.139L](#)
- Libralato, M., et al. 2016, MNRAS, 463, 1780. [2016MNRAS.463.1780L](#)
- Livingston, J. H., et al. 2018, The Astronomical Journal, 155, 115. [2018AJ....155..115L](#)
- Lomb, N. R. 1976, Astrophysics and space science, 39, 447. [1976Ap&SS..39..447L](#)
- Lovis, C., & Mayor, M. 2007, A&A, 472, 657. [2007A&A...472..657L](#)

- Majewska-Świerzbiniowicz, A., Pigulski, A., Szabó, R., & Csubry, Z. 2008. in Journal of Physics: Conference Series, Pulsating B-type stars in the young open cluster h Persei (NGC 869) (IOP Publishing), 012068. [2008JPhCS.118a2068M](#)
- Mann, A. W., et al. 2016, The Astrophysical Journal, 818, 46. [2017AJ....153...64M](#)
- Meibom, S., et al. 2013, Nature, 499, 55. [2013Natur.499...55M](#)
- Nardiello, D., et al. 2020, MNRAS, 495, 4924. [2020MNRAS.498.5972N](#)
- Obermeier, C., et al. 2016, The Astronomical Journal, 152, 223. [2016AJ....152..223O](#)
- Pasquini, L., et al. 2007, A&A, 473, 979. [2007A&A...473..979P](#)
- Percy, J. R. 1972, Publications of the Astronomical Society of the Pacific, 84, 420. [1972PASP...84..420P](#)
- Prša, A., & Zwitter, T. 2005, The Astrophysical Journal, 628, 426. [2005ApJ...628..426P](#)
- Quinn, S. N., et al. 2014, The Astrophysical Journal, 787, 27. [2014ApJ...787...27Q](#)
- Saesen, S., Briquet, M., Aerts, C., Miglio, A., & Carrier, F. 2013, The Astronomical Journal, 146, 102. [2013AJ....146..102S](#)
- Saesen, S., Carrier, F., & Pigulski, A. 2009, arXiv, 09010629. [2009CoAst.158..179S](#)
- Saesen, S., et al. 2010, A&A, 515, A16. [2010A&A...515A..16S](#)
- Santos, N. C., Israelian, G., & Mayor, M. 2004, A&A, 415, 1153. [2004A&A...415.1153S](#)
- Scargle, J. D. 1982, Astrophysical Journal, Part 1, vol 263, Dec 15, 1982, p 835-853, 263, [835. 1982ApJ...263..835S](#)
- Sokolovsky, K., & Lebedev, A. 2018, Astronomy and Computing, 22, 28. [2018A&C....22...28S](#)
- Waelkens, C., et al. 1990, Astronomy and Astrophysics Supplement Series (ISSN 0365-0138), vol 83, no 1, April 1990, p 11-25 Research supported by the Belgian Ministry of Education, 83, 11. [1990A&AS...83...11W](#)
- Zhuo, J., et al. 2021, Research in Astronomy and Astrophysics, 21, 227. [2021RAA....21..227Z](#)

## Appendix

This section presents a phaser plot of detected variable stars in our FOV of both OCs, along with their WEBDA identification numbers (top left) and estimated periods (top right).

